ELSEVIER

Volume 181, Number 1, January 2008

JOURNAL OF SOLID STATE CHEMISTRY

www.elsevier.com/locate/jssc

CONTENTS

Abstracted/indexed in BioEngineering Abstracts, Chemical Abstracts, Coal Abstracts, Current Contents/Physics, Chemical, & Earth Sciences, Engineering Index, Research Alert, SCISEARCH, Science Abstracts, and Science Citation Index. Also covered in the abstract and citation database SCOPUS®. Full text available on ScienceDirect®.

Regular Articles

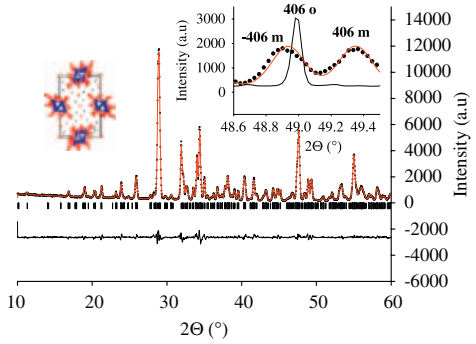

We report the synthesis, crystal structure, and electrical and magnetic properties of the novel monoclinic compounds $R_4Mo_4Mo_4O_{11}$ (R = Yb and Lu) containing infinite chains of trans-edge-sharing Mo_6 octahedra.

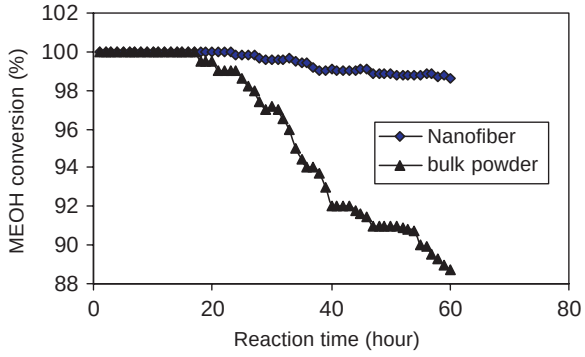

The steam reforming of methanol (SRM) to CO_2 and H_2 over La_2CuO_4 nanofiber catalyst was studied. At the temperature as low as 150 °C, methanol was completely (100%) converted to hydrogen and CO_2 without the generation of CO. Within the 60 h catalyst lifespan test, methanol conversion was maintained at 98.6% and with 100% CO_2 selectivity.

Regular Articles—Continued

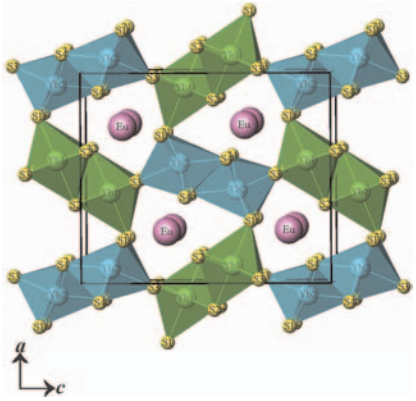

A view of the three-dimensional channel structure of $EuYb_2S_4$ down the b-axis.

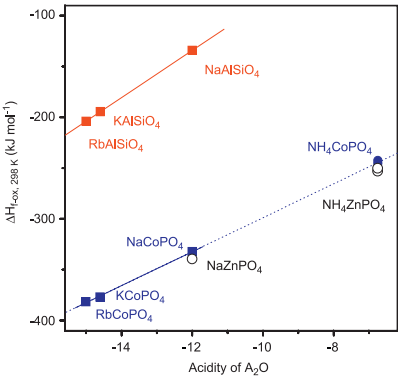

Relationship between enthalpy of formation from oxides and acid–base interaction for cobalt phosphates, zinc phosphates, and aluminosilicates with related frameworks. They exhibit similar trends, but the enthalpies of formation of phosphates are more exothermic than those of aluminosilicates because of stronger acid–base interactions.

The Heusler phases $LiRh_2Si$ and $LiRh_2Ge$: Synthesis, structure and properties

Mark S. Bailey, Qing'an Li, Emil B. Lobkovsky, D.G. Hinks and J.F. Mitchell

page 30

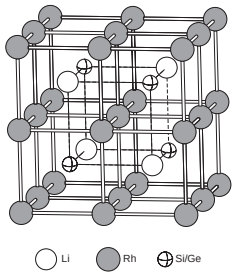

Rh, Li and either Si or Ge form an ordered coloring pattern of the bcc lattice in the Heusler phases $LiRh_2Si$ and $LiRh_2Ge$. Crystals grown from a reactive Li flux are diamagnetic metals that exhibit a T-linear resistivity above 60 K.

Trapping phosphate anions inside the $[Ag_4I]^{3+}$ framework: Structure, bonding, and properties of $Ag_4I(PO_4)$

Olga S. Oleneva, Maria A. Kirsanova, Tatiana A. Shestimerova, Nikolay S. Abramchuk, Dmitry I. Davliatshin, Mikhail A. Bykov, Evgeny V. Dikarev and Andrei V. Shevelkov

page 37

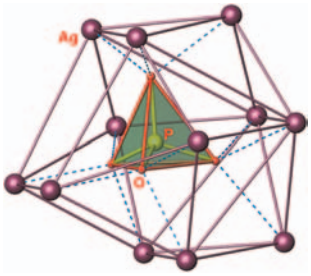

Regular $[PO_4]$ tetrahedra fill large voids in the Ag–I framework to form a host–guest compound, $Ag_4I(PO_4)$. It has a perfectly ordered crystal structure, atypical for this kind of compounds, rendering the study of the manifold Ag–Ag bonds and the host–guest interaction. However, this ordering leads to low ionic conductivity.

Long- and short-range order in stuffed titanate pyrochlores

G.C. Lau, T.M. McQueen, Q. Huang, H.W. Zandbergen and R.J. Cava

page 45

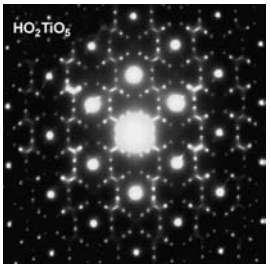

The $\langle 110 \rangle$ zone axis electron diffraction pattern for Ho_2TiO_5 reveals the coexistence of long- and short-range pyrochlore ordering. An additional complex modulation of the pyrochlore structure consisting of a seven-fold enlargement of the unit cell in the (662) direction is also observed.

Crystal structure of $Ca_{12}Al_{14}O_{32}Cl_2$ and luminescence properties of $Ca_{12}Al_{14}O_{32}Cl_2$:Eu^{2+}

Tomoyuki Iwata, Masahide Haniuda and Koichiro Fukuda

page 51

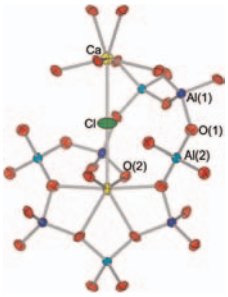

A portion of the crystal structure of $Ca_{12}Al_{14}O_{32}Cl_2$ showing eight-membered AlO_4 rings and Ca–Cl–Ca unit.

$Bi_{2/3}Ce_{1/3}Rh_2O_5$: A new mixed-valent Rh oxide with hitherto unknown structure

Hiroshi Mizoguchi, A.P. Ramirez, L.N. Zakharov, A.W. Sleight and M.A. Subramanian

page 56

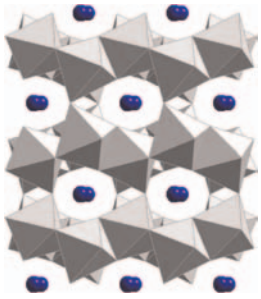

The new compound $Bi_{2/3}Ce_{1/3}Rh_2O_5$ has been discovered. The structure indicates no ordering between Rh^{3+} and Rh^{4+}. The lack of charge ordering is consistent with the metallic properties determined from electrical conductivity, Seebeck coefficient, and magnetic susceptibility measurements.

Study on the solid solution of $YMn_{1-x}Fe_xO_3$: Structural, magnetic and dielectric properties

S.L. Samal, W. Green, S.E. Lofland, K.V. Ramanujachary, D. Das and A.K. Ganguli

page 61

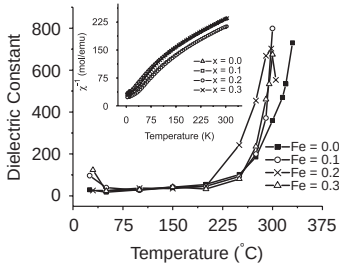

Temperature dependence of ε of $YMn_{1-x}Fe_xO_3$ ($0.0 \leqslant x \leqslant 0.3$) at 100 kHz. Inset shows the temperature variation of inverse magnetic susceptibility.

Continued

Synthesis and characterization of periodic mesoporous organosilicas from bridged organosilanes in the presence of mixed salts

Shang-Ru Zhai, I1 Kim and Chang-Sik Ha

page 67

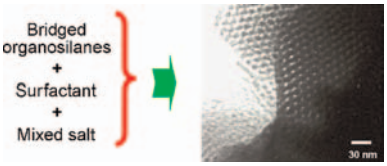

Ordered periodic mesoporous organosilicas (PMOs) could be facilely prepared with the aid of mixed salts where no extra acid was necessary.

Efficient photoluminescence of Dy^{3+} at low concentrations in nanocrystalline ZrO_2

L.A. Diaz-Torres, E. De la Rosa, P. Salas, V.H. Romero and C. Angeles-Chávez

page 75

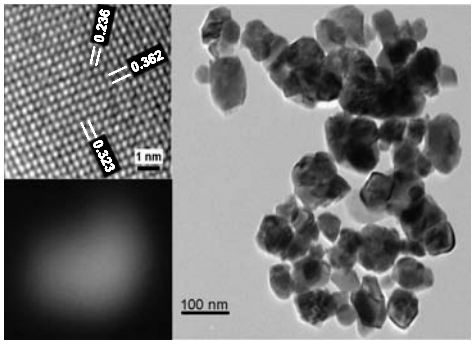

White light emission from ~70 nm ZrO_2:Dy^{3+} nanocrystals. The highest efficiency was obtained for 0.5 mol% of dopant and the dominant crystalline structure was monoclinic.

Oxidation and deprotonation of synthetic Fe^{II}–Fe^{III} (oxy)hydroxycarbonate Green Rust: An X-ray photoelectron study

M. Mullet, Y. Guillemin and C. Ruby

page 81

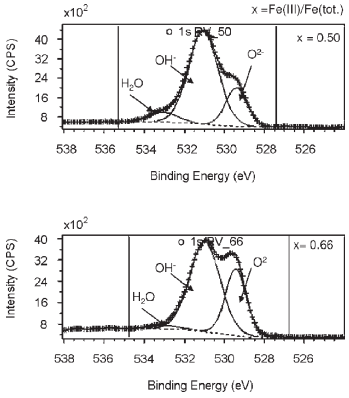

X-ray photoelectron spectroscopy (XPS) is used to investigate chemical bonding and distribution of iron and oxygen species at the surface of Green Rust (GR) compounds. First spectroscopic evidence of the deprotonation of hydroxyls groups occurring simultaneously to the oxidation of Fe(II) into Fe(III) species is provided.

Perovskite tungsten bronze-type crystals of Li_xWO_3 grown by chemical vapour transport and their characterisation

Claus H. Rüscher, Kalpana R. Dey, Tapas Debnath, Ingo Horn, Robert Glaum and Altaf Hussain

page 90

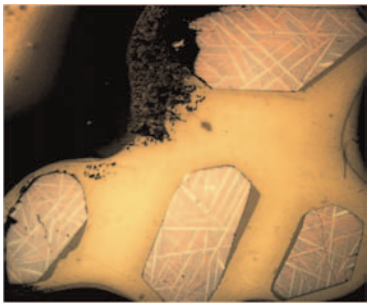

Optical microscope image (reflection mode) of Li_xWO_3 crystals of nominal composition $x = 0.35$. The separation into PTB_{cubic} (dark areas) and $PTB_{tetragonal}$ (bright areas) were used to determine the miscibility gap and optical properties.

Heat capacities, order–disorder transitions, and thermodynamic properties of rare-earth orthoferrites and rare-earth iron garnets

S.C. Parida, S.K. Rakshit and Ziley Singh

page 101

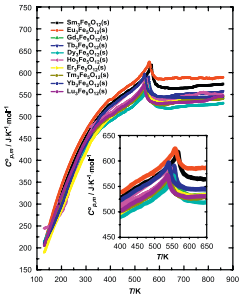

Plot of molar heat capacities ($C^o_{p,m}$) of $R_3Fe_5O_{12}$(s) (R = Sm, Eu, Gd, Tb, Dy, Ho, Er, Tm, Yb and Lu) against temperature (T). The inset shows the magnified portion of the heat capacity plot near the transition region indicating nearly same values of Curie temperatures for different $R_3Fe_5O_{12}$(s).

Synthesis and gas sensitivities of SnO_2 nanorods and hollow microspheres

Haizhen Wang, Jianbo Liang, Hai Fan, Baojuan Xi, Maofeng Zhang, Shenglin Xiong, Yongchun Zhu and Yitai Qian

page 122

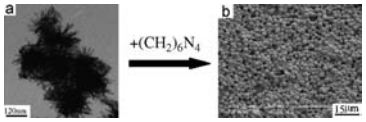

SnO_2 urchin-like structures composed of short nanorods with diameter of 10–15 nm and length of 50–70 nm and SnO_2 hollow microspheres have been synthesized via a simple H_2O_2-assisted hydrothermal method in the absence of any surfactant. With the addition of methenamine (HMT), SnO_2 hollow microspheres with diameter of 2–3 μm and shell thickness of 60–140 nm were obtained. The gas sensitivity experiments showed that the as-synthesized SnO_2 materials show good sensitivity to alcohol vapors and thus are expected to be useful in industrial applications such as gas sensors.

Synthesis and characterization of substitutional and interstitial nitrogen-doped titanium dioxides with visible light photocatalytic activity
Feng Peng, Lingfeng Cai, Hao Yu, Hongjuan Wang and Jian Yang
page 130

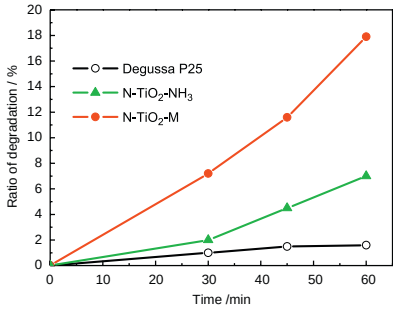

Both substitutional and interstitial N impurities can enhance the photoactivity of TiO_2 in visible light; moreover, the visible light activity of interstitial N-doped TiO_2 is higher than that of substitutional N-doped TiO_2.

First-principles investigation of $R_2O_3(ZnO)_3$ (R = Al, Ga, and In) in homologous series of compounds
Satoru Yoshioka, Kazuaki Toyoura, Fumiyasu Oba, Akihide Kuwabara, Katsuyuki Matsunaga and Isao Tanaka
page 137

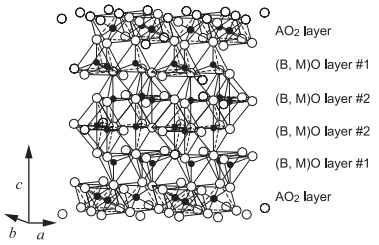

$R_2O_3(ZnO)_3$ (R = Al, Ga, and In) in homologous series of compounds are investigated using first-principles calculations with special interest on preferred occupation sites of R, relative energetics with competing phases and electronic structures.

The preparation of CdO nanowires from solid-state transformation of a layered metal-organic framework
Fang Zhang, Feng-Li Bei, Jie-Ming Cao and Xin Wang
page 143

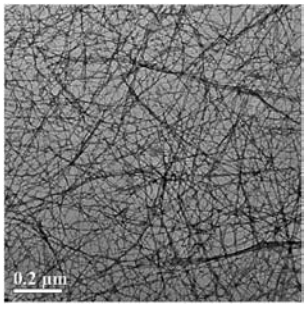

1D CdO nanowires have been prepared by an effective and reasonable complex-precursor procedure, in which a layered metal-organic framework assembled by 1D infinite zigzag chains was heated in the presence of oxygen at higher temperature.

Formation of Si–C–N ceramics from melamine–carbosilazane single source precursors
Mazin Shatnawi, Wafaa Al-Mansi and Isam Arafa
page 150

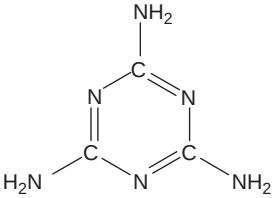

I

Pyrolysis of the prepared melamine–organosilane macromolecules afforded Si–C–N ceramics with different textural morphology.

Synthesis, stoichiometry and thermal stability of Zn_3N_2 powders prepared by ammonolysis reactions
Giordano Paniconi, Zlatka Stoeva, Ronald I. Smith, Patricia C. Dippo, Bryan L. Gallagher and Duncan H. Gregory
page 158

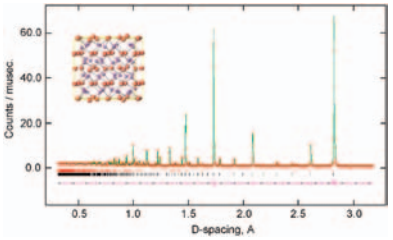

Zn_3N_2 powders prepared by careful ammonolysis reactions form with the *anti*-bixbyite structure and are almost certainly stoichiometric with no evidence for aliovalent oxygen substitution at the nitrogen sites. Zn_3N_2 cannot be described as a 100% ionic compound and PL measurements reveal a narrow band gap of approximately 0.9 eV.

Selective solution-phase synthesis of BiOCl, $BiVO_4$ and δ-Bi_2O_3 nanocrystals in the reaction system of $BiCl_3$–NH_4VO_3–NaOH
Xiang Ying Chen, Zhong Jie Zhang and Soon W. Lee
page 166

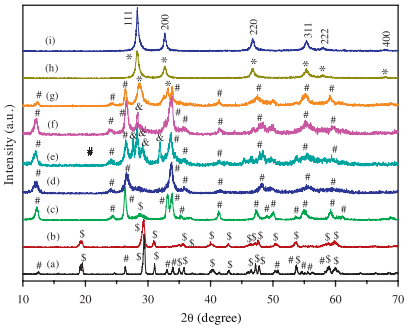

In this study, we demonstrate a straightforward solution-phase method for the selective synthesis of BiOCl, $BiVO_4$ and δ-Bi_2O_3 nanocrystals by simply manipulating the reaction temperature and the $BiCl_3$-to-NaOH mole ratio in the reaction system of $BiCl_3$–NH_4VO_3–NaOH.

Continued

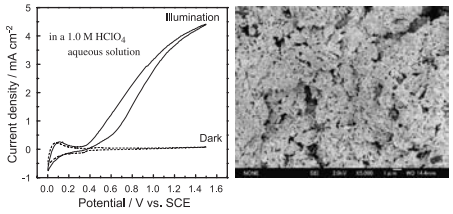

A nano-structured WO_3 platelet film was prepared by calcination from a precursor paste including suspended ammonium tungstate and polyethylene glycol. The ammonium tungstate suspension was yielded by an acid–base reaction of tungstic acid and an ammonium solution followed by deposition with ethanol addition. The photocatalytic activity of the film was 4.5–12.8 times higher than those for the other control WO_3 films prepared by similar but different procedures.

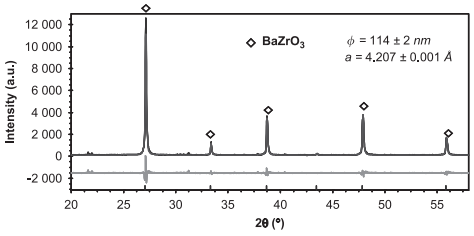

An experimental design has been conducted in order to determine the influence of the experimental parameters on the crystallinity and the grain size of $BaZrO_3$ nanopowders obtained thanks to hydrothermal synthesis in supercritical water and in a continuous way.

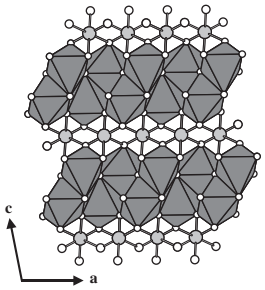

Crystal structure of $ScRe_2O_6$ in the ac-plane showing the $[Re_2O_6]_n$ layers separated by Sc-layers.

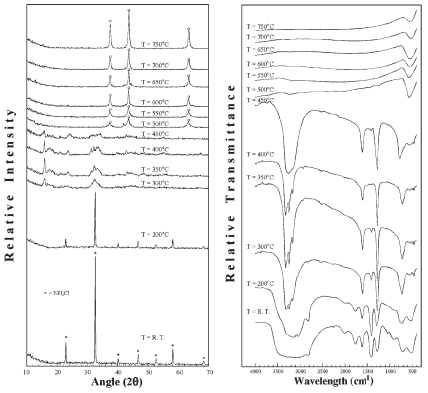

XRD and FTIR analyses of the ammonolysis of $[Cr(NH_3)_6]Cl_2$ as a function of temperature.

Rapid Communications

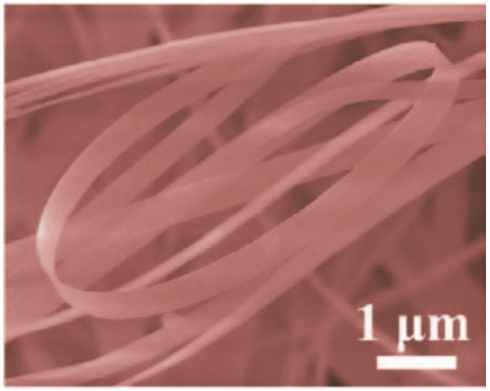

We report the mass production of very thin single-crystalline Si_3N_4 nanobelts with a high yield via catalyst-assisted pyrolysis of polymeric precursors.

Author inquiries

Submissions

For detailed instructions on the preparation of electronic artwork, consult the journal home page at http://authors.elsevier.com.

Other inquiries

Visit the journal home page (http://authors.elsevier.com) for the facility to track accepted articles and set up e-mail alerts to inform you of when an article's status has changed. The journal home page also provides detailed artwork guidelines, copyright information, frequently asked questions and more.

Contact details for questions arising after acceptance of an article, especially those relating to proofs, are provided after registration of an article for publication.

Language Polishing

Authors who require information about language editing and copyediting services pre- and post-submission should visit http://www.elsevier.com/wps/find/authorshome.authors/languagepolishing or contact authorsupport@elsevier.com for more information. Please note Elsevier neither endorses nor takes responsibility for any products, goods, or services offered by outside vendors through our services or in any advertising. For more information please refer to our Terms & Conditions at http://www.elsevier.com/wps/find/termsconditions.cws_home/termsconditions.

For a full and complete Guide for Authors, please refer to *J. Solid State Chem.,* Vol. 180, Issue 1, pp. *bmi–bmv*. The instructions can also be found at http://www.elsevier.com/wps/find/journaldescription.cws_home/622898/authorinstructions.

Journal of Solid State Chemistry has no page charges.